ELSEVIER

Journal of Membrane Science 124 (1997) 93–105

journal of MEMBRANE SCIENCE

Membrane ultrafiltration in combined hollow-fiber module systems

H.M. Yeh *, H.H. Wu

Department of Chemical Engineering, Tamkang University, Tamsui, Taiwan, ROC

Received 20 July 1995; revised 25 July 1996; accepted 26 July 1996

Abstract

A correlation equation for predicting permeate flux of membrane ultrafiltration in hollow-fiber modules has been derived based upon the resistance-in-series model with the consideration of transmembrane pressure declining along the tube axis of the hollow fibers. Ultrafiltration of a PVP-360 aqueous solution has been carried out in an Amicon model H1P30-20 hollow-fiber cartridge made of polysulfone. Correlation predictions are confirmed with the experimental results. Ultrafiltration in four combined-module systems arranged with three identical modules has been further investigated theoretically. It was found that performance in the module system arranged in series is largely better than that arranged in parallel, except for the solutions of higher feed concentrations (1.0 wt% $\leq C \leq$ 2.0 wt%) operated under low transmembrane pressure.

Keywords: Membrane ultrafiltration; Hollow-fiber module; Combined systems

1. Introduction

Ultrafiltration of macromolecular solutions has become an increasingly important separation process. Its operational pressure is usually in the range of 10 to 100 psi. The rapid development of this process was made possible by the advent of anisotropic, high-flux membranes capable of distinguishing among molecular and colloidal species in the 10^{-3} to 10 μm size range.

One of the common ultrafiltration designs is the hollow-fiber configuration in which the membrane is formed on the inside of tiny polymer cylinders fabricated into a tube-and-shell arrangement. The advantages of this arrangement are low cost of investment and operation, easy flow control and cleaning, and high specific area per unit volume. On an industrial scale, the following applications have proved to be economically attractive and useful [1]: industrial effluents, oil emulsions, wastewater, biological macromolecules, colloidal paint suspensions and medical therapeutics.

Since membrane ultrafiltration is a pressure-driven separation, the pressure applied to the working fluid provides the driving potential to force the permeate to flow through the membrane. For a small applied pressure, the permeate flux through a membrane is observed to be proportional to the applied pressure. However, as the pressure is increased, the flux begins to drop below that which would result from a linear flux–pressure behavior. Eventually a limiting

* Corresponding author. Fax: +886-26252770.

PII S0376-7388(96)00242-6

flux is reached where any further pressure increase no longer results in any increase in flux.

Ultrafiltration of macromolecular solutions is usually analyzed by the following models: (i) the gel polarization model [2–8], (ii) the osmotic pressure model [9–17], and (iii) the resistance-in-series model [18–20]. In the gel polarization model, permeate flux is reduced by the hydraulic resistance of the gel layer. In the osmotic pressure model, permeate flux reduction results from the decrease in effective transmembrane pressure that occurs as the osmotic pressure of the retentate increases. In the resistance-in-series model, permeate flux decreases due to the resistances caused by fouling or solute adsorption and concentration polarization. This method easily describes the relationships of permeate flux with operating parameters.

In industrial applications, ultrafiltration may be carried out by several hollow-fiber membrane modules connected together to enhance plant performance. Fig. 1 shows four arrangements for connecting three identical modules. The purpose of this study is to investigate, using the resistance-in-series theory, the performance of membrane ultrafiltration in combined tube-side feed hollow-fiber module systems under various feed concentrations, flow rates and transmembrane pressures.

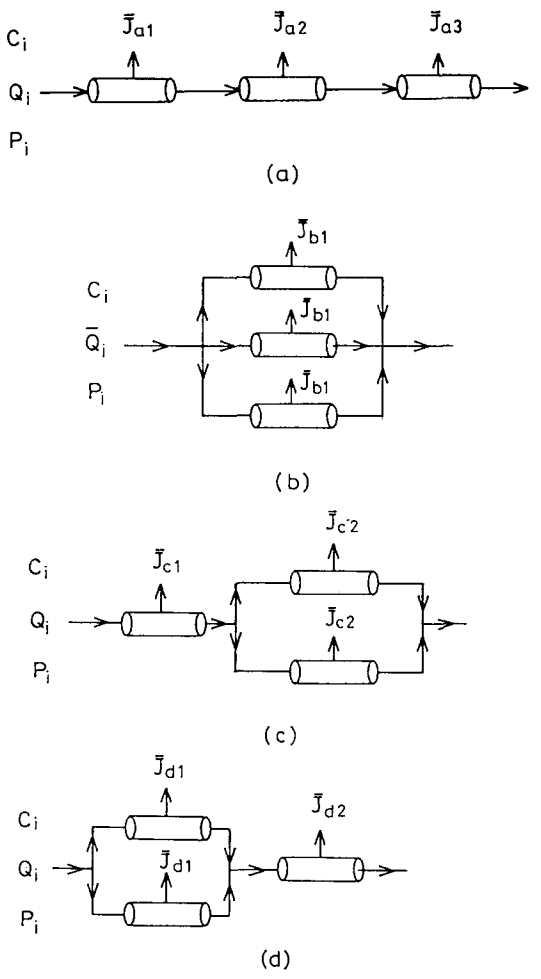

Fig. 1. Combined hollow-fiber module systems.

2. Theory

2.1. Resistance-in-series model

In the resistance-in-series model, permeate flux $J(z)$ may be expressed as

$$J(z) = \frac{\Delta P(z)}{R_m + R_f + R_p} \tag{1}$$

where R_m denotes the intrinsic resistance of a membrane, and R_p and R_f are, respectively, the resistances due to the concentration polarization/gel layer and those due to other fouling phenomena such as solute adsorption, while $\Delta P(z)$ is the transmembrane pressure defined as

$$\Delta P(z) = P(z) - P_p \tag{2}$$

In the above equation, $P(z)$ is the pressure distribution of the tube side along the axial direction, z, of a hollow fiber and P_p is the permeate pressure of the shell side which may be assumed to be constant.

R_p will be proportional to the amount and specific hydraulic resistance of the deposited layer. Since the deposited layer is compressible, R_p is function of pressure, so that we may assume

$$R_p = \phi \Delta P(z)$$

and Eq. (1) becomes

$$J(z) = \frac{\Delta P(z)}{R_m + R_f + \phi \Delta P(z)} \tag{3}$$

in which the resistances, R_m and R_f, as well as the proportional constant ϕ will be determined by ex-

perimental data. Some earlier work based on the resistance model also indicated that part of the tube side resistance is proportional to the transmembrane pressure ΔP [19,20].

Practically, Eq. (3) must satisfy the following boundary conditions,

for $\Delta P = 0$, $J = 0$;
for small ΔP, $J = (\text{const})\Delta P$;
as $\Delta P \to \infty$ (or large enough), $J = J_{\text{lim}}$ (limiting flux).

Accordingly,

$$\phi = \frac{1}{J_{\text{lim}}} \tag{4}$$

2.2. Determination of R_m, R_f and ϕ

In pure water ultrafiltration with a fresh hollow-fiber module, neither R_f nor R_p exists and the permeate flux, $J_w(z)$, for ultrafiltration of pure water is obtained from Eq. (3) as

$$J_w(z) = \frac{\Delta P(z)}{R_m} \tag{5}$$

This equation can be written with the use of average experimental values, $(\bar{J}_w)_{\text{exp}}$ and $(\overline{\Delta P})_{\text{exp}}$ as

$$\frac{1}{(\bar{J}_w)_{\text{exp}}} = \frac{R_m}{(\overline{\Delta P})_{\text{exp}}} \tag{5'}$$

Therefore, if $1/(\bar{J}_w)_{\text{exp}}$ is plotted as a function of $1/(\overline{\Delta P})_{\text{exp}}$, a straight line should result with its slope being the intrinsic resistance, R_m, of the membrane employed. In the above equation

$$(\overline{\Delta P})_{\text{exp}} = \frac{(P_i + P_L)_{\text{exp}}}{2} \tag{6}$$

in which P_i and P_L are, respectively, the inlet and outlet pressures of the tube side.

Furthermore, if experimental data obtained in ultrafiltration of an aqueous solution is also applied to Eq. (3), then

$$(\bar{J})_{\text{exp}} = \frac{(\overline{\Delta P})_{\text{exp}}}{R_m + R_f + \phi(\overline{\Delta P})_{\text{exp}}} \tag{7}$$

or

$$\frac{1}{(\bar{J}_w)_{\text{exp}}} = \phi + \frac{R_m + R_f}{(\overline{\Delta P})_{\text{exp}}} \tag{8}$$

Therefore, from a straight line plot of $1/(\bar{J}_w)_{\text{exp}}$ versus $1/(\overline{\Delta P})_{\text{exp}}$ at a certain flow velocity, u_i, and feed concentration, C_i, the values of ϕ (the intersection at the ordinate) and $(R_m + R_f)$ (the slope) as well as R_f may be determined experimentally as functions of u_i and C_i.

2.3. The pressure distribution

Since the membrane permeation rate is small compared with the volume flow rate in a hollow-fiber module, it can be assumed that the local decline in hydraulic pressure within the fiber is simply given by the Hagen–Poiseuille equation:

$$\frac{dP}{dz} = \frac{8\mu\bar{Q}}{N\pi r_m^4} = -\frac{8\mu\bar{u}}{r_m^2} \tag{9}$$

where the average volume rate in a single module of N hollow fibers, is related to $\bar{u}$ as

$$\bar{Q} = \pi r_m^2 N\bar{u} \tag{10}$$

Integrating Eq. (9) with the use of boundary condition: $P = P_i$ at $z = 0$, we have

$$P(z) = P_i - \left(\frac{8\mu\bar{Q}}{N\pi r_m^4}\right) z \tag{11}$$

The volume flow rates at the inlet and outlet of a hollow-fiber module are related to each other by

$$Q_L = Q_i - 2\pi r_m LN\bar{J} = \pi r_m^2 N_i - 2\pi r_m LN\bar{J} \tag{12}$$

in which the average permeate flux is defined as

$$\bar{J} = \frac{1}{L}\int_0^L J(z)\,dz \tag{13}$$

The percent recovery of the permeate is defined as

$$R = \frac{Q_i - Q_L}{Q_i} \times 100\% = \frac{2L\bar{J}}{r_m u_i} \times 100\% \tag{14}$$

As mentioned before, since we may assume that

$(Q_i - Q_L) \ll Q_i$, say $R < 10\%$, therefore, the arithmetic mean of volume flow rate will be taken, i.e.

$$\bar{Q} = \frac{Q_i + Q_L}{2} = Q_i - (\pi r_m LN)\bar{J} \tag{15}$$

and the pressure distribution is obtained by substituting Eq. (15) into Eq. (11). The result is

$$P(z) = P_i - \left[\left(\frac{8\mu L}{N\pi r_m^4}\right)Q_i - \left(\frac{8\mu L^2}{r_m^3}\right)\bar{J}\right]\left(\frac{z}{L}\right) \tag{16}$$

Finally, the transmembrane pressure is

$$\Delta P(z) = P(z) - P_p = \Delta P_i - \left(mQ_i - n\bar{J}\right)(z/L) \tag{17}$$

where

$$\Delta P_i = P_i - P_p \tag{18}$$

$$m = \frac{8\mu L}{N\pi r_m^4} \tag{19}$$

$$n = \frac{8\mu L^2}{r_m^3} \tag{20}$$

and the transmembrane pressure at the outlet of a hollow-fiber membrane module is

$$\Delta P_L = \Delta P_i - \left(mQ_i - n\bar{J}\right) \tag{21}$$

The assumption that the membrane permeation rate is small compared with the volume flow rate in a hollow-fiber module will be confirmed by the experimental data in Section 3.7, and for simplicity, therefore, the dependence of Q and u on z is ignored in the entire development.

2.4. Permeate fluxes of a single module

Substitution of Eq. (17) into Eq. (3) yields the expression for local permeate flux of a single hollow-fiber membrane module:

$$J(z) = \frac{\Delta P_i - \left(mQ_i - n\bar{J}\right)(z/L)}{R_m + R_f + \phi\left[\Delta P_i - \left(mQ_i - n\bar{J}\right)(z/L)\right]} \tag{22}$$

Thus, the average permeate flux of a single hollow-fiber membrane module can be obtained by substituting Eq. (22) into Eq. (13). The result is

$$\bar{J} = \frac{1}{\phi} + \frac{R_m + R_f}{\left(mQ_i - n\bar{J}\right)\phi^2}\ln\left[1 - \frac{\left(mQ_i - n\bar{J}\right)\phi}{R_m + R_f + \phi\Delta P_i}\right] \tag{23}$$

2.5. Total permeate rates of a combined-module system

Fig. 1 shows four combined-module arrangements for connecting three identical hollow-fiber membrane modules. The total permeate rates, V, in each combined-module system are expressed as follows.

2.5.1. Model a

$$V_a = \left(\bar{J}_{a1} + \bar{J}_{a2} + \bar{J}_{a3}\right)A = A\sum_{j=1}^{3}\bar{J}_{aj} \tag{24}$$

where A is the total surface area of one hollow-fiber module. According to Eq. (23),

$$\bar{J}_{aj} = \frac{1}{\phi} + \frac{R_m + R_f}{\left\{m(Q_i)_{aj} - n\bar{J}_{aj}\right\}\phi^2} \times \ln\left[1 - \frac{\left\{m(Q_i)_{aj} - n\bar{J}_{aj}\right\}\phi}{R_m + R_f + \phi(\Delta P_i)_{aj}}\right] \quad j = 1, 2, 3 \tag{25}$$

in which the volume rates and transmembrane pressures at the inlet of each module are, according to Eqs. (12) and (21):

$$(Q_i)_{a1} = Q_i \tag{26}$$

$$(Q_i)_{a2} = (Q_L)_{a1} = Q_i - A\bar{J}_{a1} \tag{27}$$

$$(Q_i)_{a3} = (Q_L)_{a2} = (Q_i)_{a2} - A\bar{J}_{a2} = \left(Q_i - A\bar{J}_{a1}\right) - A\bar{J}_{a2} \tag{28}$$

$$(\Delta P_i)_{a1} = \Delta P_i \tag{29}$$

$$(\Delta P_i)_{a2} = (\Delta P_L)_{a1} = \Delta P_i - \left(mQ_i - n\bar{J}_{a1}\right) \tag{30}$$

$$(\Delta P_i)_{a3} = (\Delta P_L)_{a2} = (\Delta P_i)_{a2} - \left\{m(Q_i)_{a2} - n\bar{J}_{a2}\right\} = \left\{\Delta P_i - \left(mQ_i - n\bar{J}_{a1}\right)\right\} - \left\{m\left(Q_i - A\bar{J}_{a1}\right) - n\bar{J}_{a2}\right\} \tag{31}$$

2.5.2. Model b

$$V_b = 3\bar{J}_{b1}A \tag{32}$$

Since

$$(Q_i)_{b1} = Q_i/3 \tag{33}$$

$$(\Delta P_i)_{b1} = \Delta P_i \tag{34}$$

therefore, according to Eq. (23),

$$\bar{J}_{b1} = \frac{1}{\phi} + \frac{R_m + R_f}{\left\{(mQ_i/3) - n\bar{J}_{b1}\right\}\phi^2} \times \ln\left[1 - \frac{\left\{(mQ_i/3) - n\bar{J}_{b1}\right\}\phi}{R_m + R_f + \phi(\Delta P_i)}\right] \tag{35}$$

2.5.3. Model c

$$V_c = \left(\bar{J}_{c1} + 2\bar{J}_{c2}\right)A \tag{36}$$

where

$$\bar{J}_{c1} = \bar{J}_{a1} \tag{37}$$

$$\bar{J}_{c2} = \frac{1}{\phi} + \frac{R_m + R_f}{\left\{m(Q_i)_{c2} - n\bar{J}_{c2}\right\}\phi^2} \times \ln\left[1 - \frac{\left\{m(Q_i)_{c2} - n\bar{J}_{c2}\right\}\phi}{R_m + R_f + \phi(\Delta P_i)_{c2}}\right] \tag{38}$$

$$(Q_i)_{c2} = (Q_i)_{a2}/2 \tag{39}$$

$$(\Delta P_i)_{c2} = (\Delta P_i)_{a2} \tag{40}$$

2.5.4. Model d

$$V_d = \left(2\bar{J}_{d1} + \bar{J}_{d2}\right)A \tag{41}$$

where

$$\bar{J}_{dj} = \frac{1}{\phi} + \frac{R_m + R_f}{\left\{m(Q_i)_{dj} - n\bar{J}_{dj}\right\}\phi^2} \times \ln\left[1 - \frac{\left\{m(Q_i)_{dj} - n\bar{J}_{dj}\right\}\phi}{R_m + R_f + \phi(\Delta P_i)_{dj}}\right] \tag{42}$$

in which

$$(Q_i)_{d1} = Q_i/2 \tag{43}$$

$$(Q_i)_{d2} = 2(Q_L)_{d1} = 2\left\{(Q_i)_{d1} - A\bar{J}_{d1}\right\} = Q_i - 2A\bar{J}_{d1} \tag{44}$$

$$(\Delta P_i)_{d1} = \Delta P_i \tag{45}$$

$$(\Delta P_i)_{d2} = (\Delta P_L)_{d1} = \Delta P_i - \left\{m(Q_i)_{d1} - n\bar{J}_{d1}\right\} = \Delta P_i - \left\{(mQ_i/2) - n\bar{J}_{d1}\right\} \tag{46}$$

3. Experimental

3.1. Apparatus and materials

The flow diagram of an ultrafiltration apparatus with a single hollow-fiber membrane module is shown in Fig. 2. An Amicon model H1P30-20 hollow-fiber cartridge (Amicon, Danvers, MS) was employed for membrane ultrafiltration. The fibers (r_m = 0.025 cm, L = 15.3 cm, N = 250, A = 600 cm^2) were made of polysulfone.

An aqueous solution of polyvinylpyrrolidone (PVP)-360 (Sigma, M_n = 360,000) was used as a

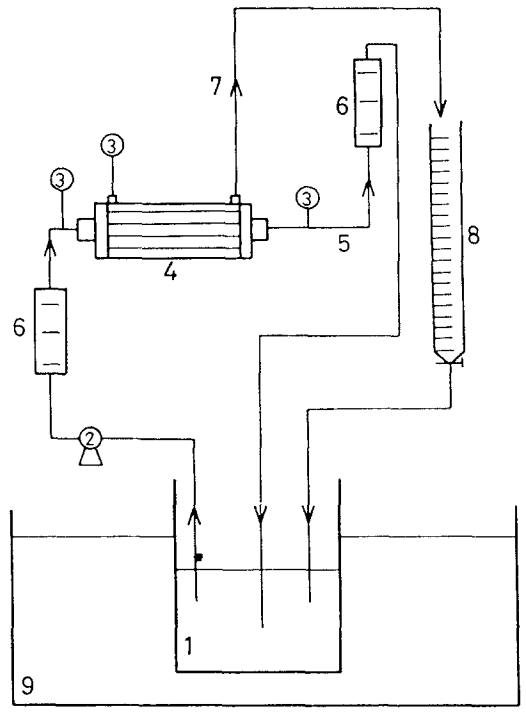

Fig. 2. Flow diagram of experimental apparatus. 1: feed tank; 2: pump; 3: pressure gauge; 4: hollow-fiber module; 5: concentrate; 6: flow meter; 7: permeate; 8: collector; 9: thermostat.

Table 1
Experimental data of permeate flux for pure water with u_i = 0.1684 m/s

$(\overline{\Delta P})_{exp} \times 10^{-5}$ (Pa)	$(\bar{J}_w)_{exp} \times 10^6$ (m^3/m^2·s)
0.9384	194.9
0.7421	153.9
0.5602	113.9
0.3639	75.70
0.1724	34.64

test solution for ultrafiltration. The solvent was pure ion exchange water.

The feed solution was circulated by a high-pressure pump with a variable speed motor (L-07553-20, Cole-Parmer, Chicago, IL), and the feed flow was measured with a flowmeter (L-03217-34, Cole-Parmer). The pressure was measured by a pressure transmitter (Model 891.14.425, Wika).

3.2. Experimental conditions and procedure

The experimental conditions were as follows. The feed concentrations, C_i, were 0.1, 0.5, 1.0 and 2.0 wt% PVP-360; the feed flow velocities, u_i, were 0.0723, 0.1209, 0.1684 and 0.2195 m/s; and the feed transmembrane pressures, ΔP_i were 19, 38, 57, 77, 96, and 115 kPa. The temperature of the feed solution in all experiments was kept at 25°C using a thermostat. During a run, both permeate and retentate were recycled back to the feed tank to keep the feed concentration constant.

The experimental procedure was as follows. First, a fresh hollow-fiber module was used for the determination of the intrinsic resistance of membrane,

Table 2
Experimental data of PVP-360 aqueous solution

C_i (wt%)	u_i = 0.0723 m/s		u_i = 0.1209 m/s		u_i = 0.1684 m/s		u_i = 0.2195 m/s	
	$\overline{\Delta P} \times 10^{-5}$ (Pa)	$\bar{J} \times 10^6$ (m^3/m^2·s)	$\overline{\Delta P} \times 10^{-5}$ (Pa)	$\bar{J} \times 10^6$ (m^3/m^2·s)	$\overline{\Delta P} \times 10^{-5}$ (Pa)	$\bar{J} \times 10^6$ (m^3/m^2·s)	$\overline{\Delta P} \times 10^{-5}$ (Pa)	$\bar{J} \times 10^6$ (m^3/m^2·s)
0.1	1.063	6.300	1.049	8.346	1.039	10.01	1.044	11.38
	0.8714	5.959	0.8523	7.810	0.8474	9.570	0.8618	10.71
	0.6799	5.781	0.6607	7.540	0.6655	8.999	0.6607	9.894
	0.4884	5.434	0.4788	6.731	0.4740	7.815	–	–
	0.2969	4.540	–	–	–	–	–	–
0.5	1.063	3.559	1.053	4.969	1.039	6.214	1.039	7.380
	0.8714	3.472	0.8618	4.960	0.8475	6.065	0.8475	7.181
	0.6799	3.428	0.6703	4.755	0.6560	5.884	0.6560	6.828
	0.4884	3.224	0.4788	4.441	0.4644	5.418	0.4644	6.075
	0.2969	2.780	0.2921	3.676	0.2825	4.209	0.2729	4.726
	0.1101	1.931	–	–	–	–	–	
1.0	1.044	2.790	1.044	4.228	1.025	5.229	1.010	6.205
	0.8523	2.768	0.8523	4.179	0.8331	5.101	0.8187	5.930
	0.6607	2.704	0.6607	4.035	0.6464	4.922	0.6320	5.746
	0.4740	2.518	0.4740	3.724	0.4549	4.384	0.4405	5.186
	0.2021	2.221	0.2825	3.092	0.2633	3.436	0.2538	3.776
	0.1005	1.466	–	–	–	–	–	–
2.0	1.001	1.679	0.9289	1.953	0.8666	2.486	0.7948	2.391
	0.7996	1.504	0.7421	1.720	0.6751	2.013	0.6129	2.148
	0.6033	1.316	0.5506	1.469	0.4884	1.618	0.4309	1.747
	0.4309	1.054	0.3783	1.129	0.3208	1.129	0.2586	1.112
	0.2490	0.8907	0.1963	0.6621	–	–	–	–

R_m. Permeate fluxes for ultrafiltration of pure water $(\bar{J}_w)_{exp}$ were measured at $u_i = 0.1684$ m/s and under various inlet transmembrane pressures $(\overline{\Delta P})_{exp}$. Then the feed water was replaced with the test solution. Permeate fluxes for PVP-360 solution $(\bar{J})_{exp}$ were measured under all operating conditions at steady state. Values of permeate flux reached steady state within 30 to 120 min.

After each solution run, the membrane module was cleaned by a combination of high circulation and backflushing with pure water. The cleaning procedure was repeated until the original water flux had been restored.

3.3. Determination of R_m

The experimental data of the permeate flux for pure water, $(\bar{J}_w)_{exp}$, with $u_i = 0.1684$ m/s and various $(\overline{\Delta P})_{exp}$ are presented in Table 1. With the use of Table 1, it was found that a straight line of $1/(\bar{J}_w)_{exp}$ versus $1/(\overline{\Delta P})_{exp}$ could be constructed by the least-squares method. Thus, the intrinsic resistance of the hollow-fiber membrane module employed in this study can be determined by Eq. (5) coupled with the use of Table 1. Under various transmembrane pressure, $(\overline{\Delta P})_{exp}$, the measured value of the intrinsic resistance for the membrane system used in the present study was

$$R_m = 0.501 \times 10^9 \ (\text{Pa} \cdot \text{s/m}) \tag{47}$$

3.4. Determination of ϕ and R_f

The experimental data of solution permeate flux, $(\bar{J})_{exp}$, are given in Table 2. It was found with the use of Table 2 that at a certain inlet fluid velocity u_i and feed concentration, C_i, a straight line of $1/(\overline{\Delta J})_{exp}$ versus $1/(\overline{\Delta P})_{exp}$ could be constructed by the least-squares method. According to Eq. (8), the intersection at ordinate, ϕ, and the slope of this straight line, $(R_m + R_f)$, may be determined [20]. All values determined are listed in Table 3. It is noted that R_f is determined by

$$R_f = (R_m + R_f) - 0.501 \times 10^9 \ (\text{Pa} \cdot \text{s/m}) \tag{48}$$

3.5. Correlation equations for ϕ and R_f

It is observable from the experimental results that ϕ is a function of mean velocity and solution concentration. Since the permeate across the membrane wall is small compared with the flow rates through the tubes, the mean velocity and solution concentration which are still unknown before prediction, are very close to the inlet velocity and feed concentration, respectively. For simplicity, therefore, we may assume [20,21]

$$\phi = \alpha_1 u_i^{\alpha_2} C_i^{\alpha_3} \tag{49}$$

in which α_1, α_2, and α_3 are constants and their values were determined with the use of Table 3. The correlation equation for ϕ thus obtained is

$$\phi = 4 \times 10^4 u_i^{-0.77} C_i^{0.30} \ (\text{s/m}) \tag{50}$$

It is seen from Table 3 that R_f is nearly indepen-

Table 3
The fitting parameter of experimental data for PVP-360 system

C_i (wt%)	u_i (m/s)	$(R_m + R_f) \times 10^{-9}$ (Pa·m²·s/m³)	$R_f \times 10^{-9}$ (Pa·m²·s/m³)	$\phi \times 10^{-5}$ (s/m)
0.1	0.0723	2.445	1.944	1.369
	0.1209	2.424	1.923	0.9755
	0.1684	2.458	1.957	0.7552
	0.2195	2.359	1.858	0.6555
0.5	0.0723	2.934	2.433	2.531
	0.1209	2.951	2.450	1.683
	0.1684	3.001	2.500	1.274
	0.2195	2.866	2.365	1.051
1.0	0.0723	3.847	3.346	3.164
	0.1209	3.456	2.955	1.989
	0.1684	3.613	3.112	1.517
	0.2195	3.518	3.017	1.219
2.0	0.0723	24.81	24.30	3.503
	0.1209	24.87	24.37	2.381
	0.1684	24.29	23.79	–
	0.2195	–	–	–

$R_m = 0.501 \times 10^9$ (Pa·m²·s/m³).

dent of crossflow velocity but varies very sensitively with feed concentration, thus, we may assume [20,21]

$$R_r = \beta_1 \exp(\beta_2 \sinh C_i) \quad (51)$$

The values of the constants β_1 and β_2 were also determined with the use of Table 3. The correlation equation for R_f is

$$R_f = 1.61 \times 10^9 e^{0.73 \sinh C_i} \text{ (Pa} \cdot \text{s/m)} \quad (52)$$

The goodness of fit of Eqs. (50) and (52) as well as Eq. (23) to the experimental data will be discussed in the next two sections.

3.6. Comparison of correlation predictions of a single membrane module with experimental results

From the dimensions of the module used, $r_m = 2.5 \times 10^{-4}$ m, $L = 0{,}153$ m, $N = 250$ and $A = 0.06$ m^2. In addition, the viscosity of PVP-360 aqueous solution at 25°C may be estimated by [20]

$$\mu = 0.894 \times 10^{-3} e^{0.875 C_i} \text{ (Pa} \cdot \text{s), or (kg/m} \cdot \text{s)} \quad (53)$$

Thus, from Eqs. (10), (19) and (20),

$$Q_i = \pi r_m^2 L u_i N = 7.5 \times 10^{-6} u_i \text{ (m}^3\text{/s)} \quad (54)$$

$$u_i = 1.33 \times 10^5 Q_i \quad (55)$$

$$m = 3.56 \times 10^8 e^{0.875 C_i} \text{ (Pa} \cdot \text{s/m}^3\text{)} \quad (56)$$

$$n = 1.07 \times 10^7 e^{0.875 C_i} \text{ (Pa} \cdot \text{s/m)} \quad (57)$$

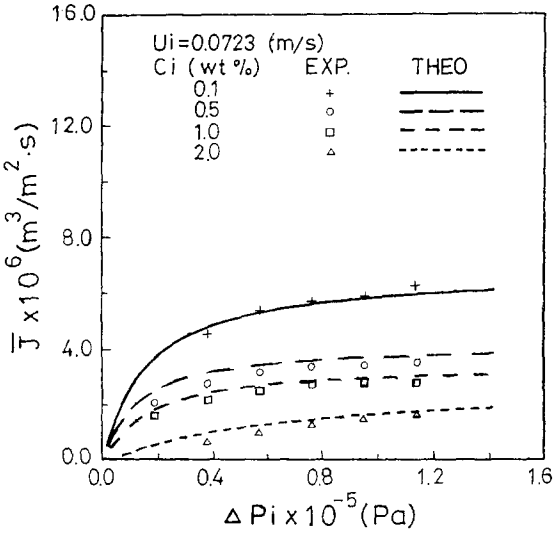

Fig. 3. Relation between $\bar{J}$ and ΔP_i for $u_i = 0.0723$ m/s.

Table 4
The percent recovery of the permeate

C_i (wt%)	u_i (m/s)	$\overline{\Delta P} \times 10^{-5}$ (Pa)	$J \times 10^6$ (m^3/m^2·s)	R(%)
2.0	0.2195	0.2586	1.112	0.6201
2.0	0.0723	0.2490	0.8907	1.508
0.1	0.2195	1.044	11.38	6.346
0.1	0.0723	1.063	6.300	10.67

Correlation predictions of permeate fluxes under various u_i, C_i and ΔP_i were calculated from Eqs. (23), (47), (50), (52), (54)–(57). Fig. 3 shows the good agreement between calculated and measured results for an inlet velocity of 0.0723 m/s. Other inlet velocities show similar agreements.

3.7. The percent recovery of permeate

Since $r_m = 2.5 \times 10^{-4}$ m and $L = 0.153$ m, Eq. (14) becomes

$$R = 1224(\bar{J}/u_i) \times 100\% \quad (58)$$

Some typical values of the percent recovery of permeate R were then calculated with the use of Table 2. The results are shown in Table 4. It is seen in Table 4 that R is small enough to ignore the dependence of Q and u on z in the entire development. Similarly, the calculation of ϕ and R_f may neglect the effect of permeate flux on the flow velocity.

4. Performance of combined-module arrangement

4.1. Calculation of ϕ and R_f

Consider the ultrafiltration of PVP-360 aqueous solutions in the four combined module systems shown in Fig. 1. Each combined-module systems is arranged with three Amicon model H1P30-20 hollow-fiber cartridges. The equations derived in Section 2.5 will be employed here for calculating the total permeation rate of a combined-module system. Due to the small percent recovery, the following approxima-

tions obtained from Eq. (55) were used to calculate ϕ and R_f from Eqs. (50) and (52):

$$(u_i)_{aj} = 1.33 \times 10^5 Q_i, \quad j = 1, 2, 3 \tag{59}$$

$$(u_i)_{b1} = (1/3)(u_i)_{aj} = 4.44 \times 10^4 Q_i \tag{60}$$

$$(u_i)_{c1} = (u_i)_{aj} = 1.33 \times 10^5 Q_i \tag{61}$$

$$(u_i)_{c2} = (1/2)(u_i)_{aj} = 6.67 \times 10^4 Q_i \tag{62}$$

$$(u_i)_{d1} = (1/2)(u_i)_{aj} = 6.67 \times 10^4 Q_i \tag{63}$$

$$(u_i)_{d2} = (u_i)_{aj} = 1.33 \times 10^5 Q_i \tag{64}$$

4.2. Calculation of total permeate rates

The total permeate rates, V, of a combined-module system under various feed concentrations, flow rates, Q_i, and transmembrane pressures, ΔP_i, are calculated from Eqs. (24)–(47), (50), (52), (56), (57), (59)–(64), and the results are shown in Figs. 4 and 5.

4.3. Results and discussion

Rising fluid velocity in the fiber tubes has two conflicting effects. One, the decrease in resistance to permeation due to reduction in concentration polarization, is good for ultrafiltration, while the other, the decrease in average transmembrane pressure due to increase in frictional pressure loss, is bad for ultrafiltration. It appears, therefore, that proper adjustment of fluid velocity as well as proper arrangement of a combined-module system might effectively suppress any undesirable resistance to permeation due to concentration polarization while still maintaining a reasonable transmembrane pressure and thereby lead to improved permeate recoveries.

For a specified volumetric feed rate, fluid velocities in the fiber tubes for each combined-module system are quite different. For example, the velocity in the system arranged in series (model a shown in Fig. 1) is three times that in the system arranged in parallel (model b shown in Fig. 1). Therefore, fluid velocities in the combined module systems can be adjusted and controlled by proper physical arrangement of the modules.

It can be seen from Figs. 4 and 5 that feed concentration, cross-flow velocity and transmembrane pressure all have a significant effect on the performance of each combined-module system. As will be described in more detail below, the configuration which has the greatest productivity changes with variation in the operating parameters.

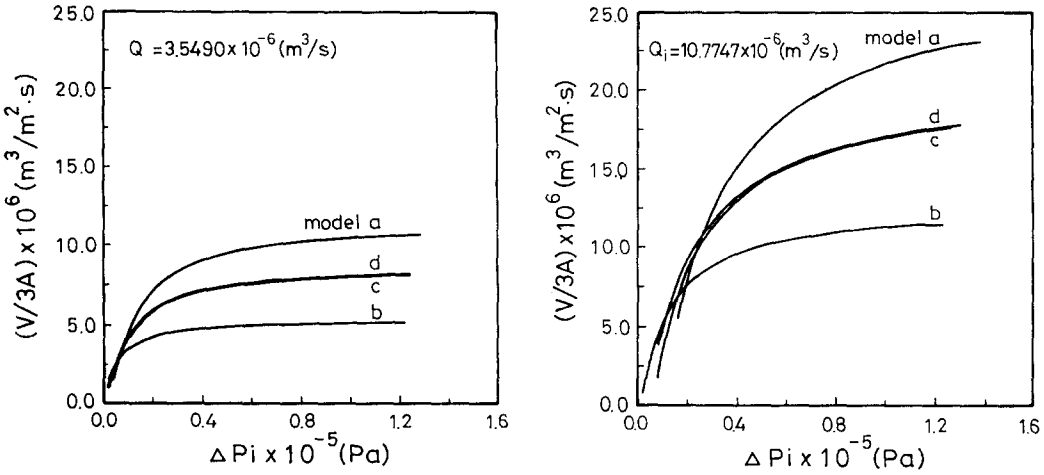

Fig. 4. Relation between $(V/3A)$ and ΔP_i for $C_i = 0.1$ wt%, PVA-360.

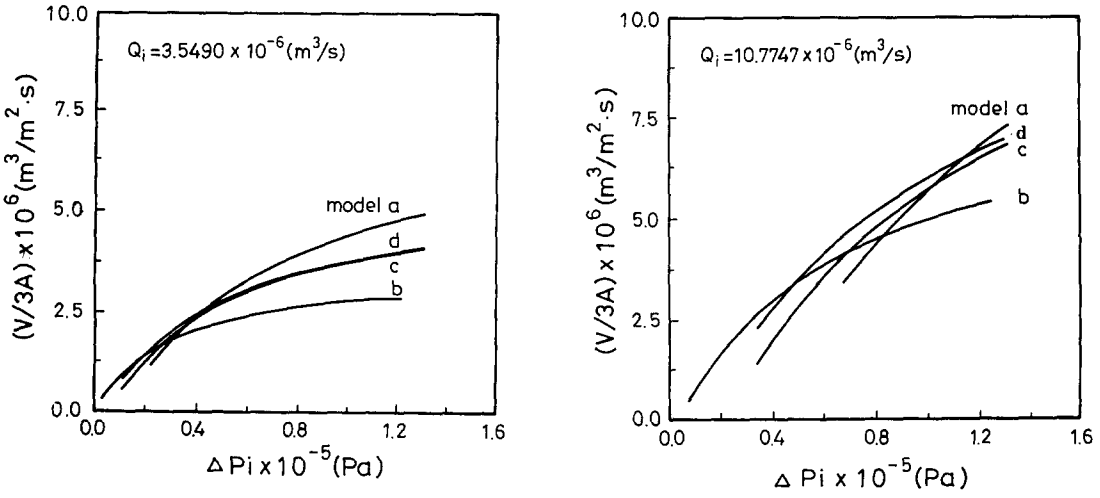

Fig. 5. Relation between $(V/3A)$ and ΔP_i for $C_i = 2.0$ wt%, PVA-360.

4.3.1. Lower feed concentration

It is found from Fig. 4 that in the region of lower feed concentration ($C_i = 0.1$ wt%), the order of performance among the four combined-module systems shown in Fig. 1 is

$$V_a > V_d \approx V_c > V_b \tag{65}$$

The reason why the combine-module system arranged in series (model a) performs better than that arranged in parallel (model b) is that, as mentioned earlier, the higher velocity produced in model a will decrease permeation resistance. Although the average transmembrane pressure in model a is lower due to the higher fluid velocity, the reduction is compensated by the decreased resistance. This may be demonstrated by considering an example from Fig. 4 such that

$$C_i = 0.1 \text{ wt\%}, \qquad Q_i = 10.8 \times 10^{-6} \text{ m}^3/\text{s}$$

$$\Delta P_i = 1.2 \times 10^5 \text{ Pa}$$

$$V_a/3A = 34.2 \times 10^{-6} \text{ m}^3/\text{m}^2 \cdot \text{s}$$

$$V_b/3A = 18.2 \times 10^{-6} \text{ m}^3/\text{m}^2 \cdot \text{s}$$

The average transmembrane pressure in model a is then calculated from Eq. (21) with L replaced by $3L$ and with the use of Eqs. (56) and (57), as

$$\begin{aligned}\overline{\Delta P}_a &= \left[\Delta P_i + (\Delta P_{3L})_a\right]/2 \\ &= \Delta P_i - \left[3mQ_i - 3^2 n(V_a/3A)\right]/2 \\ &= 1.155 \times 10^5 \text{ Pa}\end{aligned} \tag{66}$$

while that in model b is also calculated from Eq. (21) but with Q_i replaced by $Q_i/3$, as

$$\begin{aligned}\overline{\Delta P}_b &= \left[\Delta P_i + (\Delta P_L)_b\right]/2 \\ &= \Delta P_i - \left[mQ_i/3 - n(V_b/3A)\right]/2 \\ &= 1.194 \times 10^5 \text{ Pa}\end{aligned} \tag{67}$$

Accordingly, their corresponding permeation resistances are

$$\sum_i R_{a,i} = \frac{\overline{\Delta P}_a}{V_a/3A} = 3.38 \times 10^9 \text{ Pa} \cdot \text{s/m} \tag{68}$$

$$\sum_i R_{b,i} = \frac{\Delta P_b}{V_b/3A} = 6.56 \times 10^9 \text{ Pa} \cdot \text{s/m} \tag{69}$$

4.3.2. Higher feed concentration

Although transmembrane pressure will decrease more for ultrafiltration of solutions of higher concentration ($C_i = 2.0$ wt%) whose viscosity is higher,

especially for operation at the high fluid velocities created in model a, Fig. 5 shows that under higher transmembrane-pressure operation, say $\Delta P_i > 0.4 \times 10^5$ Pa in Fig. 5,

$$V_a > V_d \approx V_c > V_b \tag{70}$$

This result indicates that for operation under higher transmembrane pressure, the reduction of transmembrane pressure is compensated for by decreased resistance. As an illustration, let us take the data in Fig. 5 as follows:

$C_i = 2$ wt%, $\quad Q_i = 10.8 \times 10^{-6}$ m^3/s

$\Delta P_i = 1.2 \times 10^5$ Pa

$V_a/3A = 6.76 \times 10^{-6}$ m^3/m$^2 \cdot$ s

$V_b/3A = 5.34 \times 10^{-6}$ m^3/m$^2 \cdot$ s

With the use of Eqs. (56), (57), (66)–(69), we have

$\Delta P_a = 0.887 \times 10^5$ Pa,

$\sum_i R_{a,i} = 1.31 \times 10^{10}$ Pa $\cdot$ s/m

$\Delta P_b = 1.16 \times 10^5$ Pa,

$\sum_i R_{b,i} = 1.84 \times 10^{10}$ Pa $\cdot$ s/m

On the other hand, for lower transmembrane pressures, say $\Delta P_i < 0.4 \times 10^5$ Pa in Fig. 5, the reduction of effective transmembrane pressure can not be compensated for by decreased resistance. Therefore,

$$V_b > V_d > V_c > V_a \tag{71}$$

This may be demonstrated by considering an example from Fig. 5 such that

$C_i = 2$ wt%, $\quad Q_i = 10.8 \times 10^{-6}$ m^3/s

$\Delta P_i = 0.4 \times 10^5$ Pa

$V_a/3A = 1.08 \times 10^{-6}$ m^3/m$^2 \cdot$ s

$V_b/3A = 3 \times 10^{-6}$ m^3/m$^2 \cdot$ s

Again, with the use of Eqs. (56), (57), (66)–(69), one obtains

$\overline{\Delta P}_a = 0.087 \times 10^5$ Pa,

$\sum_i R_{a,i} = 8.06 \times 10^9$ Pa $\cdot$ s/m

$\overline{\Delta P}_b = 0.365 \times 10^5$ Pa,

$\sum_i R_{b,i} = 1.23 \times 10^{10}$ Pa $\cdot$ s/m

5. Conclusion

A correlation equation, Eq. (23), for predicting the permeate flux for ultrafiltration in a hollow-fiber module has been derived based on the resistance-in-series model including consideration of decline in transmembrane pressure along the tube axis of the hollow fibers. Ultrafiltration of an aqueous PVP-360 (polyvinylpyrrolidone) solution in an Amicon model H1P30-20 hollow-fiber cartridge made of polysulfone, has been carried out for various feed concentrations, transmembrane pressures and feed flow rates.

As expected, permeate flux increases as transmembrane pressure or fluid velocity increases, but decreases when feed concentration increases. It is shown in Table 3 that the fouling layer resistance R_f is nearly independent of crossflow velocity u_i but varies very sensitively with feed concentration C_i. Further, the limiting permeate flux, J_{lim} (or $1/\phi$), increases with crossflow velocity but decreases when feed concentration increases.

Ultrafiltration in the four combined-module systems arranged with three identical modules has also been investigated theoretically. It was found that the performance of the module system arranged in series (model a) was largely better than that arranged in parallel (model b), except for solutions of higher feed concentrations ($C_i = 2.0$ wt%) operated under lower transmembrane pressures ($\Delta P_i < 0.4 \times 10^5$ Pa). It is also noted that the performances of model c and model d are almost the same, except for solutions at higher concentrations operated under low transmembrane pressures in which case $V_d > V_c$.

6. List of symbols

A	total surface area of a hollow-fiber module (m^2)
C_i	concentration of feed solution (wt% of PVP-360)
J	volume permeate flux of solution (m^3/m$^2 \cdot$ s)
$\bar{J}$	average value of J in a hollow-fiber module (m^3/m$^2 \cdot$ s)
J_{lim}	limiting flux (m^3/m$^2 \cdot$ s)

J_w volume permeate flux of pure water ($m^3/m^2 \cdot s$)
L length of hollow fiber (m)
m constant defined by Eq. (19) ($Pa \cdot s/m^3$)
N number of hollow fibers in a membrane module
n constant defined by Eq. (20) ($Pa \cdot s/m$)
P pressure distribution on the tube side (Pa)
P_i pressure at the inlet of a hollow fiber (Pa)
P_L pressure at the outlet of a hollow fiber (Pa)
P_p permeate pressure on the shellside (Pa)
ΔP transmembrane pressure, $P - P_p$ (Pa)
$\overline{\Delta P}$ arithmetic-mean transmembrane pressure (Pa)
ΔP_i $P_i - P_p$ (Pa)
ΔP_L $P_L - P_p$ (Pa)
Q_i volume flow rate at the inlet of a hollow-fiber module (m_3/s)
Q_L volume flow rate at the outlet of a hollow-fiber module (m_3/s)
Q average volume flow rate in a hollow-fiber module (m^3/s)
R_f resistance due to solute adsorption and fouling ($Pa \cdot s/m$)
R_m intrinsic resistance of membrane ($Pa \cdot s/m$)
R_p resistance due to concentration polarization/gel layer ($Pa \cdot s/m$)
$\Sigma_i R_i$ total permeation resistance ($Pa \cdot s/m$)
r_m inside radius of hollow fiber (m)
u_i mean axial velocity at fiber inlet (m/s)
$\bar{u}$ average axial velocity through the fiber tube (m/s)
V total volume permeate rate in a combined-fiber module system (m^3/s)
z axial coordinate (m)

6.1. Greek letters

μ viscosity of solution ($Pa \cdot s$)
ϕ $1/J_{lim}$ ($m^2 \cdot s/m^3$)

6.2. Subscripts

a,b,c,d model a, b, c, d
1,2,3 module number

Acknowledgements

The authors wish to express their thanks to the Chinese National Science Council for financial aid.

References

[1] M.C. Porter, Membrane filtration, in P.A. Schweitzer (Ed.), Handbook of Separation Techniques for Chemical Engineers, McGraw-Hill, New York, 1979, sect. 2.1.
[2] W.F. Blatt, A. Dravid, A.S. Michales and L. Nelsen, Solute polarization and cake formation in membrane ultrafiltration: causes, consequences, and control techniques, in J.E. Filnn (Ed.), Membrane Science and Technology, Plenum Press, New York, 1970, p. 47.
[3] M.C. Porter, Concentration polarization with membrane ultrafiltration, Ind. Eng. Chem. Proc. Res. Dev., 11 (1972) 234.
[4] R.B. Grieves, D. Bhattacharyya, W.G. Schomp and J.L. Bewley, Membrane ultrafiltration of a nonionic surfactant, AIChE J., 19 (1973) 766.
[5] J.J.S. Shen and R.F. Probstein, On the prediction of limiting flux in laminar ultrafiltration of macromolecular solutions, Ind. Eng. Chem. Fundam., 16 (1977) 459.
[6] S. Nakao, T. Nomura and S. Kimura, Characteristics of Macromolecular gel layer formed on ultrafiltration tubular membrane, AIChE J., 25 (1979) 615.
[7] A.G. Fane, C.J.D. Fell and A.G. Waters, The relationship between membrane surface pore characteristics and flux for ultrafiltration membranes, J. Membr. Sci., 9 (1981) 245.
[8] A.G. Fane, Ultrafiltration of suspensions, J. Membr. Sci. 20 (1984) 249.
[9] J.G. Wijmans, S. Nakao and C.A. Smolders, Flux limitation in ultrafiltration: osmotic pressure model and gel layer model, J. Membr. Sci., 20 (1984) 115.
[10] A.A. Kozinski and E.N. Lightfoot, Protein ultrafiltration: a general example of boundary layer filtration, AIChE J., 18 (1972) 1030.
[11] W. Leung and R.F. Probstein, Low polarization in laminar ultrafiltration of macromolecular solutions, Ind. Eng. Chem. Fundam., 18 (1979) 274.
[12] R.P. Wendt, E. Klein, F.F. Holland and K.E. Eberle, Hollow fiber ultrafiltration of calf serum and albumin in the Pregel uniform-wall-flux region, Chem. Eng. Commun., 8 (1981) 251.
[13] S. Nakao and S. Kimura, Models of membrane transport phenomena and their applications for ultrafiltration data, J. Chem. Eng. Jpn., 15 (1982) 200.
[14] C. Kleinstreuer and M.S. Paller, Laminar dilute suspension flows in plate-and-frame ultrafiltration units, AIChE J., 29 (1983) 529.
[15] M.J. Clifton, N. Abidine, P. Aptel and V. Sanchez, Growth of the polarization layer in ultrafiltration with hollow-fiber membranes, J. Membr. Sci., 21 (1984) 233.

[16] R.P. Gooding Ma, C.H. Gooding and W.K. Alexander, A dynamic model for low-pressure, hollow-fiber ultrafiltration, AIChE J., 31 (1985) 1728.
[17] H. Nabetani, M. Nakajima, A. Watanabe, S. Nakao and S. Kumura, Effects of osmotic pressure and adsorption on ultrafiltration of ovalbumin, AIChE J., 36 (1990) 907.
[18] B.H. Chiang and M. Cheryan, Ultrafiltration on skim milk in hollow fibers, J. Food Sci., 51 (1986) 340.
[19] M. Assadi and D.A. White, A model for determining the steady state flux of inorganic microfiltration membrane, Chem. Eng. J., 48 (1992) 11.
[20] H.M. Yeh and T.W. Cheng, Resistance-in-series for membrane ultrafiltration in hollow fiber of tube-and-shell arrangement, Sep. Sci. Technol., 28 (1993) 1341.
[21] T.W. Cheng, Hollow-fiber membrane ultrafiltration, Ph.D. thesis, National Taiwan University, Taipei, Taiwan, ROC, 1992.